Mon. Not. R. Astron. Soc. **279,** 257–274 (1996)

Morphologies in megaparsec-size powerful radio galaxies

Ravi Subrahmanyan,[1,4,5] Lakshmi Saripalli[2,4,5] and Richard W. Hunstead[3]

[1]*Raman Research Institute, Sadashivanagar, Bangalore 560 080, India*
[2]*Indian Institute of Astrophysics, Koramangala, Bangalore 560 034, India*
[3]*Astrophysics Department, School of Physics, University of Sydney, NSW 2006, Australia*
[4]*Australia Telescope National Facility, CSIRO, PO Box 76, Epping, NSW 2121, Australia*
[5]*Astronomy Institutes of the University of Bonn, Universität Bonn, Auf dem Hügel 71, D-53121 Bonn 1, Germany*

Accepted 1995 October 4. Received 1995 October 4; in original form 1995 August 2

ABSTRACT

We present radio images with the Australia Telescope of a sample of powerful radio galaxies. The observations were designed to be sensitive to the largest-scale structures in the radio sources. The morphologies are representative of radio galaxies with FR II type structures and with sizes exceeding 1 Mpc. We observe the giant sources to have the same axial ratios as those in smaller sources with similar radio powers. Moreover, the deviations from axial symmetry are also observed to be linearly scaled from sources an order of magnitude smaller. The observations are indicative of self-similar evolution in the morphologies of powerful radio galaxies.

Key words: galaxies: active – intergalactic medium – radio continuum: galaxies.

1 INTRODUCTION

The morphologies of radio lobes represent the interaction between beams emanating from active galactic nuclei and from the ambient medium. In powerful radio galaxies with FR II morphology (Fanaroff & Riley 1974) the beams propagate with small losses until they interact strongly with the ambient medium at hotspots located at the ends of the radio source. Relativistic particles reaccelerated at these hotspots fill a cocoon, which interacts with the ambient medium at a contact discontinuity, and often appears to surround the beams and form a bridge of emission linking the hotspots to the central core: this is basically the beam model for powerful radio galaxies (Scheuer 1974; Begelman, Blandford & Rees 1984). The radio lobes and bridges in powerful radio galaxies represent dynamical states in their evolution, and variations in the morphological properties with linear size and radio powers are, therefore, probes of the temporal evolution in this class of objects.

Observations of relatively low-power FR II radio galaxies, with 178-MHz radio powers $P_{178} < 10^{27}$ W Hz^{-1} sr^{-1}, have shown that bridges are common in these classical double radio sources and that two-thirds of these sources have distorted bridges that deviate from an axially symmetric configuration (Leahy & Williams 1984). Examples of extreme distortions in the form of large wings are also seen in the low-power FR II sources imaged by Black et al. (1992). Higher-power sources tend to have a greater contrast between the hotspots and the lower-surface-brightness bridges (Jenkins & McEllin 1977), and detections of bridges in these as well (Leahy, Muxlow & Stephens 1989) suggested that the centrally directed tails from hotspots are generally not docked and that bridges are ubiquitous. The bridges sometimes become relatively faint towards the central core; nevertheless, the bridge radio power tends to increase with increasing source power. The above-mentioned observations also show that sources tend to become more elongated and bridge distortions less pronounced with increasing radio power.

Baldwin (1982) considered the distribution of a complete sample of radio sources in the *P–D* (radio power versus linear extent) diagram. The distribution appeared fairly uniform over linear sizes in the range 100–500 kpc, but showed a sharp decline in numbers beyond 500 kpc. The distribution is indicative of monotonicity in the evolution of sources up to about 500 kpc and evolution in a different regime thereafter. The morphological studies mentioned above have been restricted to samples of sources with median extents of a few hundred kpc. A comparison of the morphological properties of these smaller sources with that of giant-size sources beyond the break at ≈ 500 kpc may provide clues to the cause of the change in evolution.

The bridges in giant-size powerful radio galaxies may be useful probes of the intergalactic medium (Subrahmanyan & Saripalli 1993) because most of the radio lobes, in those >1 Mpc sources which are located in the field, fall well outside the commonly observed X-ray haloes surrounding isolated elliptical galaxies. Observations of the representa-

tive morphologies of the giant sources, a comparison with smaller-sized sources, and a modelling of the evolution in the powerful radio galaxies will naturally constrain the properties of the intergalactic medium (IGM) as well.

In this paper, we report our observations of sources we believe to be representative of the largest FR II radio structures, those with sizes $\gtrsim 1$ Mpc. We compare their morphologies with smaller sources of similar powers and examine the optical fields as an indicator of the environment. This study does not consider the giant sources known in the literature (cf. Saripalli et al. 1986; Saripalli 1988) which are not included by the selection criteria adopted below. The implications for models of radio source evolution are discussed in a later paper. Herein we adopt an Einstein–de Sitter cosmology with Hubble constant $H_0 = 50$ km s^{-1} Mpc^{-1}.

2 SOURCE SAMPLE SELECTION

Our sources are a subset of the *confirmed MRC extended sample* of Jones & McAdam (1992; hereinafter referred to as JM) imaged with the Molonglo Observatory Synthesis Telescope (MOST). Their sources have declinations $< -30°$ and form a complete sample, confirmed to be extended and not confused, for angular extents ≥ 1.5 arcmin and 843-MHz flux densities ≥ 1 Jy. Large sources with low surface brightness may still, however, be excluded.

Our observations were made with the Australia Telescope Compact Array (ATCA; see The Australia Telescope 1992). The minimum antenna spacing in this telescope is 31 m, and synthesized images at the lowest operating frequency of 1.4 GHz would be sensitive to structures with angular extents at most ≈ 12 arcmin. Therefore, we restricted our sample to sources with total angular size ≤ 12 arcmin. The longest baselines of the ATCA provide a resolution of about 10 arcsec at 1.4 GHz. We assumed the typical source width to be a fifth of its extent, and restricted our sample to sources ≥ 3 arcmin in extent so that their bridges would be well resolvable with at least 4 beams across. Good resolution of the bridges is necessary to distinguish any amorphous components from jets and bright ridges; the amorphous components may be less transitory and more useful as probes of the ambient medium. The sample selection criteria have been chosen to ensure that the interferometric synthesized images would reproduce all structural components in the sample sources, with no missing large-scale features, down to the sensitivity and resolution limits.

Only sources with linear extents ≥ 750 kpc were included, so that our sample would be representative of giant sources, and the large-scale morphology would represent the interaction of the lobes with the IGM. We rejected sources whose parent galaxies were members of rich clusters or located in crowded fields, to ensure that our sample consisted only of field galaxies whose large-scale environment is the IGM and not any intracluster medium. We further restricted the sample to include only sources with an FR II edge-brightened morphology. The bridges in these sources are expected to be the oldest and most relaxed parts in double radio sources and, therefore, the parts most likely to be in equilibrium with any ambient medium.

The sources constituting our sample are listed in Table 1. We also list the b_J magnitudes (as estimated by JM from a comparison with reference images of galaxies of known magnitude) of the suggested optical identifications (IDs), redshifts z (estimated in some cases from the magnitudes), 843-MHz flux densities (S_{843}) and the total source angular extents (LAS). The 843-MHz flux densities listed here were based on improved calibration of the earlier MOST data obtained by JM. The flux densities and largest angular sizes at 1376 MHz (S_{1376}) were measured from the ATCA images described below.

3 OBSERVATIONS

All the sources were observed during 1992 June–October in three array configurations of the ATCA: an extended 6.0A, an intermediate 1.5D and a compact 0.375 km. Every source was observed in each configuration at about eight different hour angles; these individual scans were of 10-min duration and were accompanied by a 4-min observation on a nearby unresolved calibrator. Useful data were obtained in 49 frequency channels of 1-MHz width, covering the band from 1351 to 1399 MHz.

The calibration and imaging were performed using the NRAO AIPS routines. The complex gains of the array elements were determined using nearby calibrators. Bandpass calibration was also done for the source data using the observations of their respective calibrators. The overall flux-density scale was set by bootstrapping the visibility amplitudes to observations of PKS B1934 – 638; the flux density of this primary calibrator was adopted to be 15.0 Jy at 1376 MHz. All the channel data were gridded together and imaged using the AIPS routine MX and the images were deconvolved using APCLN. Because we combined data from compact and extended arrays, the synthesized beams had the shape of a narrow profile mounted on an extended pedestal. Consequently, residual emission that was not deconvolved tended to appear as spurious extended emission features that could contribute significant flux density. We performed the CLEAN deconvolution to sufficient depth to ensure that these residuals were below the image noise levels. All the images were corrected for the attenuation due to the primary-beam patterns of the array elements.

All eight sources are presented in Figs 1(a)–8(a) as contour representations and separately as grey-scale images in Figs 1(b)–8(b). The images have been smoothed so that the effective beams are circular; the grey-scale representations correspond to images with larger smoothing and consequently lower resolutions. The half-maximum profiles of the synthesized beams corresponding to the contour representations are indicated by the circles in the bottom right-hand corners of the contour plots: these beam sizes span the range 8–12 arcsec FWHM.

4 NOTES ON INDIVIDUAL SOURCES

The properties of the sources, derived from the images at 1376 MHz, are given in Table 2. The linear extents of the sources (D), the radio powers (P_{1376}, in W Hz^{-1} sr^{-1}) and the spectral indices, α_{843}^{1376} (we define $S_\nu \sim \nu^{-\alpha}$), computed between 843 MHz and 1376 MHz are listed. The estimation of axial ratios (R_N, R_S and R_T) and energy densities (u_N, u_S and u_T) is described in Sections 6 and 7 respectively.

Table 1. Observed properties of the sources in the sample.

Source	b_J	z	S_{843} (Jy)	S_{1376} (Jy)	LAS (arcmin)
0114−476	17.0	0.146	5.48	2.97	11.7
0211−479	19.5	0.2195	1.65	1.26	6.3
0424−728	19.0	0.1921*	3.27	1.66	4.1
0511−305	16.0	0.0583	4.90	3.24	11.4
0707−359	20.0	0.2182*	3.42	2.01	8.2
1545−321	17.5	0.1085	3.58	1.64	8.3
1910−800	> 22.0	0.346	1.48	0.82	6.1
2356−611	17.0	0.0964	32.3	24.7	6.5

*Redshifts inferred from b_J magnitudes.

Table 2. Derived properties of the sources.

Source	D (Mpc)	$\log P_{1376}$	α_{843}^{1376}	R_N	R_S	R_T	u_N (10^{-14} J m^{-3})	u_S (10^{-14} J m^{-3})	u_T (10^{-14} J m^{-3})
0114−476	2.35	25.38	1.25	–	1.8	4.1	2.6	3.0	2.8
0211−479	1.71	25.32	0.55	3.9	3.7	7.6	1.6	4.8	3.2
0424−728	1.01	25.39	1.38	2.5	1.7	4.0	9.3	11	9.9
0511−305	1.05	24.58	0.84	4.0	1.6	5.0	1.7	2.3	2.0
0707−359	2.21	25.56	1.08	3.0	3.0	5.9	7.2	6.3	6.6
1545−321	1.32	24.87	1.59	4.1	6.8	10.3	15	12	13
1910−800	2.20	25.61	1.21	4.9	3.9	8.5	13	12	12
2356−611	0.93	25.90	0.55	–	2.6	5.3	12	16	13

Cross symbols in all the contour images (Figs 1a–8a) indicate the positions of the optical IDs. For all the sources except 1910 − 800 we show the position of the optical ID suggested by JM. In the case of 1910 − 800 the cross symbol locates the optical object that appears coincident with the radio core we have detected. 843-MHz MOST images of all the sources were presented in JM along with references to previous work. Measurements of the core emission in these sources are presented in Jones, McAdam & Reynolds (1994). Below, we examine the morphologies observed in the 1376-MHz images and discuss the applicability of standard theories – proposed for the origin of the observed morphologies in sources which are an order of magnitude smaller in linear size – for these giant radio galaxies.

4.1 0114 − 476 (Fig. 1)

We detect an unresolved core component at the position of the optical ID suggested in JM, with linear jet-like structures issuing from this core towards each of the lobes. The jets show large contrasts in intensity along their lengths and appear to have unusually pronounced wiggles. There are no bright hotspots at the extremities of the radio lobes. The jet towards the northern lobe appears to be indistinguishable after it enters the lobe, but it probably curves through a large angle and ends in a well-resolved emission plateau along the north-west edge of this lobe. The southern beam appears to end in an elongated knot located about a third of the distance to the extremity of the southern lobe; this knot component is the brightest in the entire source. However, we detect a faint compact component along the jet axis and two-thirds of the distance to the end of the southern lobe and this suggests continuity of the beam to the broad emission plateau at the southern end of the source. A peculiar linear feature is observed almost perpendicular to the jet axis and intersecting the source between the core and the bright knot in the southern jet. There is an emission gap between the core and the northern lobe; no corresponding gap is seen towards the southern lobe. The boundaries of both lobes are sharply defined, which could indicate that they are confined and not in free expansion.

The radio luminosity places this source in the FR II category and the source indeed has an edge-brightened morphology. The jet-to-counterjet ratio, measured as the intensity ratio between the brightest knots in the two sides, is 8, and the contrast in the jets, defined as the intensity ratio between the knot and interknot regions, is > 4. These properties of the jet are consistent with those in FR II sources. The fractional flux in the core is 0.2 per cent (at 1376 MHz) and this low core fraction is characteristic of powerful radio galaxies. There are, however, no hotspots at the ends of the source and the jets appear to terminate in very diffuse emission with low surface brightness, a characteristic of sources in the FR I category. Hotspots in the lobes are the brightest components in FR II sources and consequently would also be the most short lived, expanding and disappearing if the beams should turn off. We speculate, therefore, that 0114 − 476 may be an example of a source where the beams have been interrupted. The 'rejuvenated' beams may initially be terminating in the cocoon that is a remnant of past activity. Such a picture may explain the very steep overall spectrum and the FR I type structures.

We have searched, unsuccessfully, for an optical galaxy along the linear radio structure perpendicular to the axis of 0114 − 476, in an attempt to identify it as a separate radio source. This structure, seen also by JM in the MOST image, has a projected separation from the 0114 − 476 host galaxy of 110 kpc. If we speculate that this orthogonal structure

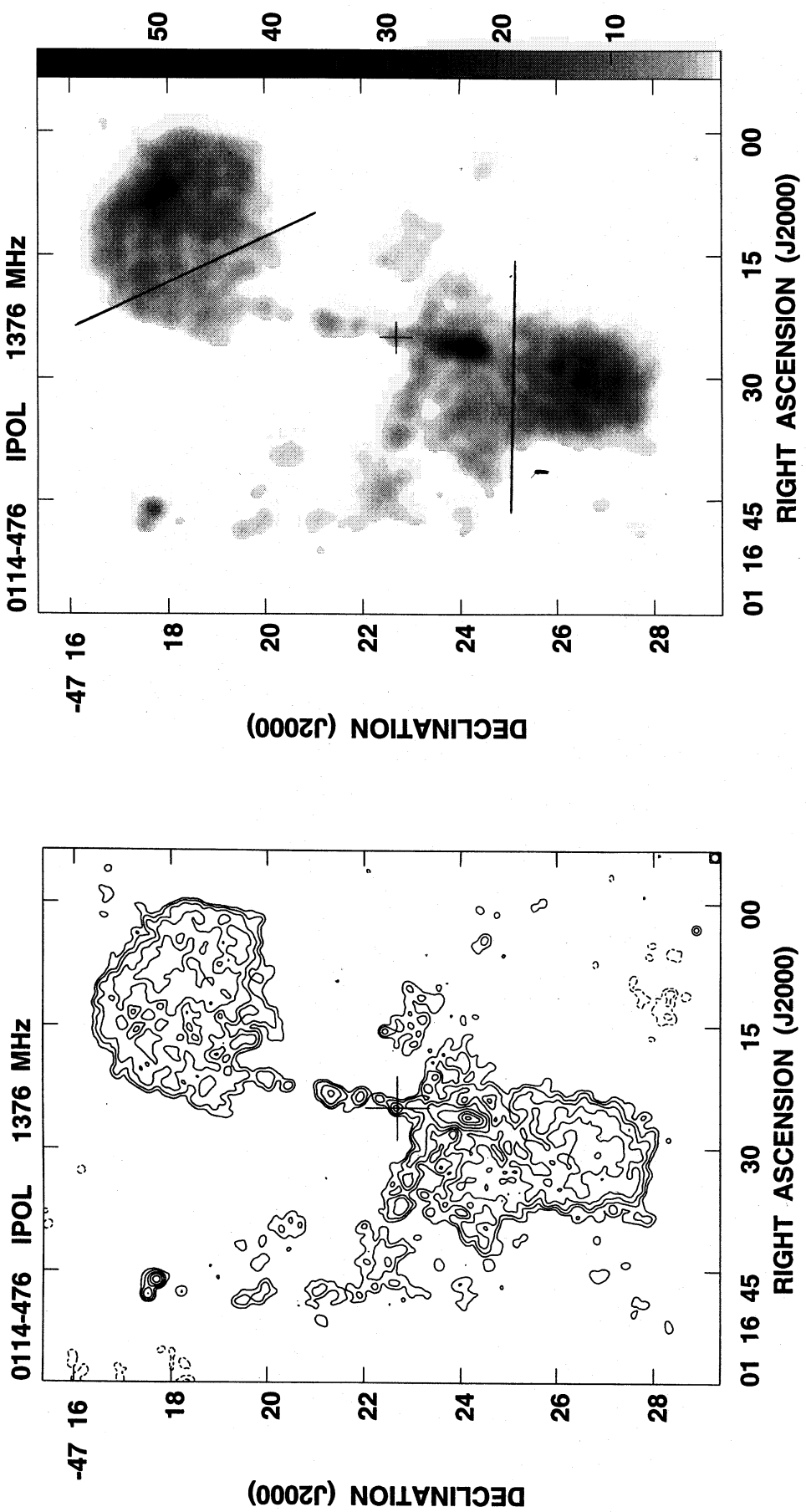

Figure 1. 1376-MHz images of 0114 – 476 in the form of (a) contours and (b) grey-scales. The cross symbol marks the position of the galaxy identification. Contours are at levels of 1 mJy beam^{-1} × (−1, −0.5, 0.5, 1, 2, 4, 8, 16, 24, 32) and the beam size is 10 arcsec FWHM. The grey-scale spans the range 0.5–60 mJy beam^{-1} with a beam smoothed to 15 arcsec FWHM.

represents an axis of past activity in the same parent galaxy, which has then moved away, the relic axis would have an unusually large age. We are led to conclude, therefore, that the peculiar linear feature represents an interaction of the backflow from the southern lobe with some discontinuity in the ambient medium. We plan to study the spectral index distribution over the source to investigate this hypothesis further.

4.2 0211 − 479 (Fig. 2)

The source has the double-lobed morphology, with hotspots at the ends, which is typical of powerful radio galaxies. We have also detected a weak core component coincident with the proposed optical ID. The radio trail from the southern hotspot is directed along the source axis and almost all the way to the core. Close to the core, however, there appears to be a sharp bend towards the west, away from the source axis. The backflow from the brighter northern hotspot is initially directed towards the core, but appears to be deflected abruptly, again towards the west; this is also seen in the MOST map of JM. A gap in emission is seen between the core and the northern lobe.

The brightness immediately behind the hotspots and towards the core appears to go through a minimum on both sides of the source, and this may be indicating temporal variations in the beam power.

Departures from axial symmetry have been suggested as arising from the interaction between backflowing material from the hotspots with gaseous haloes around the parent galaxies (Leahy & Williams 1984). The bend in the northern lobe occurs, however, about 600 kpc (in projection) from the parent galaxy, and the gaseous coronae observed around early-type galaxies in X-rays usually extend no further than ≈ 100 kpc (Forman, Jones & Tucker 1985). Moreover, the bend is only on the northern side, with little evidence for a corresponding interaction on the southern side.

The twin-beam model for powerful radio sources (Begelman et al. 1984) expects the lobe region closest to the core to be the site where the beam initially deposited its energy. Offsets in this lobe section from the source axis are sometimes interpreted as due to movement of the relic lobe with respect to the parent galaxy during the source lifetime, perhaps driven by pressure gradients in the ambient medium or due to the motion of the parent galaxy (cf. Ekers et al. 1983). The observed offset in 0211 − 479 is about 300 kpc and requires a relative velocity of $0.01ct_8^{-1}$, where t_8 is the age of the source in units of 10^8 yr. First, the required velocity would be markedly higher than the peculiar velocities typical of field galaxies, unless the source age exceeds 10^9 yr. Secondly, it exceeds the expected sound speed in any photoionized IGM (Miralda-Escudé & Rees 1994) by two orders of magnitude; therefore, buoyancy effects in the IGM are also not expected to be the cause of the departure from axial symmetry in this giant source.

4.3 0424 − 728 (Fig. 3)

The northern lobe in this source has an unresolved hotspot at the end, but the southern lobe, though edge brightened, has no compact hotspot. We have detected a possible weak core component at the position of the suggested optical ID. The bridge in this source is continuous with no emission gaps. The southern lobe appears symmetric about the source axis, but the bridge joining the northern hotspot to the core seems to be displaced to the east of this axis and the magnitude of the offset is ≈ 125 kpc close to the core.

The presence of a hotspot in the northern end of the source and the possible detection of a core component are indicative of continued activity in the central engine. The absence of a hotspot at the southern end may, however, indicate asymmetry and/or variability in the beams, or asymmetry in the ambient environments at the two ends of the source.

4.4 0511 − 305 (Fig. 4)

Bolton, Clarke & Ekers (1965) suggested the galaxy at the position marked 'a' in Figs 4(a) and (b) as the parent galaxy of the radio source. Subsequently, Searle & Bolton (1968) failed to detect emission lines from this galaxy and as a consequence Schilizzi & McAdam (1975) suggested two other fainter galaxies (at positions marked 'b' and 'c') as possible IDs. Ekers et al. (1989), however, report the detection of a radio core at the position marked 'a' based on their 5-GHz VLA snapshot observations of the source. In addition, JM note the presence of a 'wisp' to the west from galaxy 'a'. An optical image of galaxy 'a', extracted from the digitized archives of the SERC IIIaJ southern sky survey plates, is shown in Fig. 4(c). The galaxy has a very disturbed and peculiar morphology: the isophotes appear to deviate strongly from elliptical. It is also extremely large, with a halo extending > 80 kpc along the minor axis. As pointed out by JM, there is a prominent extension to the west that appears to curve to the south; this feature extends to about 100 kpc from the nucleus of the parent galaxy. Within this extension is a bright star-like object that might be the nucleus of an interacting companion. Inspection of a deep red UK Schmidt plate of the field shows that the tail to the west is relatively less prominent than on the blue-sensitive IIIaJ survey plate. All these features point to 'a' being the parent galaxy; it has a redshift of $z = 0.0583$ (P. Shaver, private communication).

No core component is detected in our image of this source at the position of the optical ID. The radio source has hotspots at the extreme ends and cometary bridges extending almost to the centre of the source. The two lobes appear to be separated by a narrow gap in emission. The overall morphology is inversion symmetric; however, the centrally directed tail from the north-east hotspot is straight whereas that from the south-west hotspot curves through a large angle and appears to be deflected towards the east. The linear dimensions of the departures from axial symmetry well exceed that of observed galactic haloes; these suggest that a changing beam axis, which swings through $\gtrsim 90°$, could be responsible for the inversion symmetry (cf. Ekers 1982).

4.5 0707 − 359 (Fig. 5)

The source has bright hotspots at the ends and an unresolved core component. There are two hotspots in the south-east lobe and the line joining these is almost orthogo-

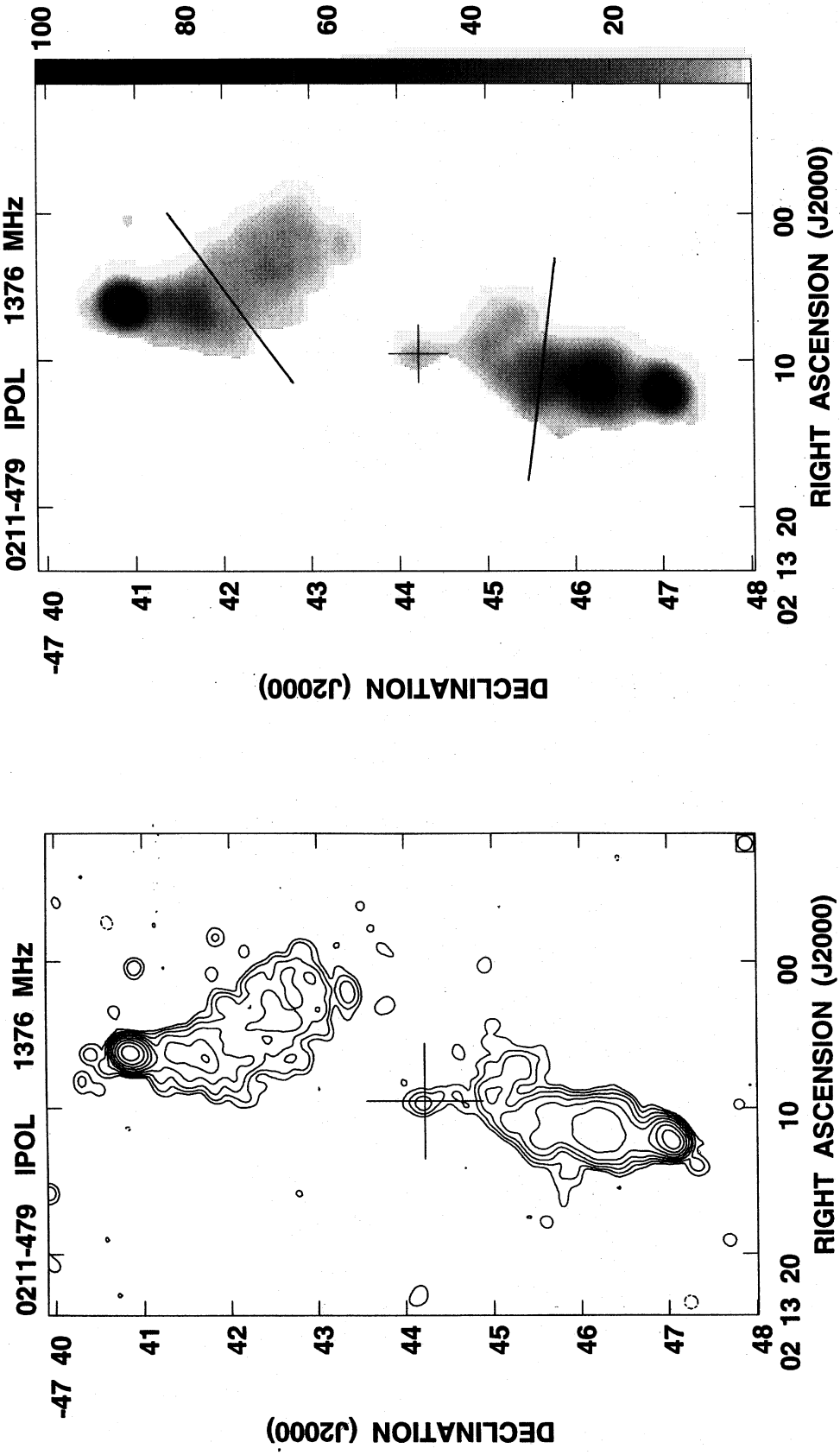

Figure 2. 1376-MHz images of 0211 − 479, as for Fig. 1. Contours are at 1 mJy beam^{-1} × (−0.5, 0.5, 1, 2, 4, 8, 16, 32, 64, 128), and the beam size is 10 arcsec FWHM. The grey-scale spans the range 0.5–100 mJy beam^{-1} with a beam of 15 arcsec FWHM.

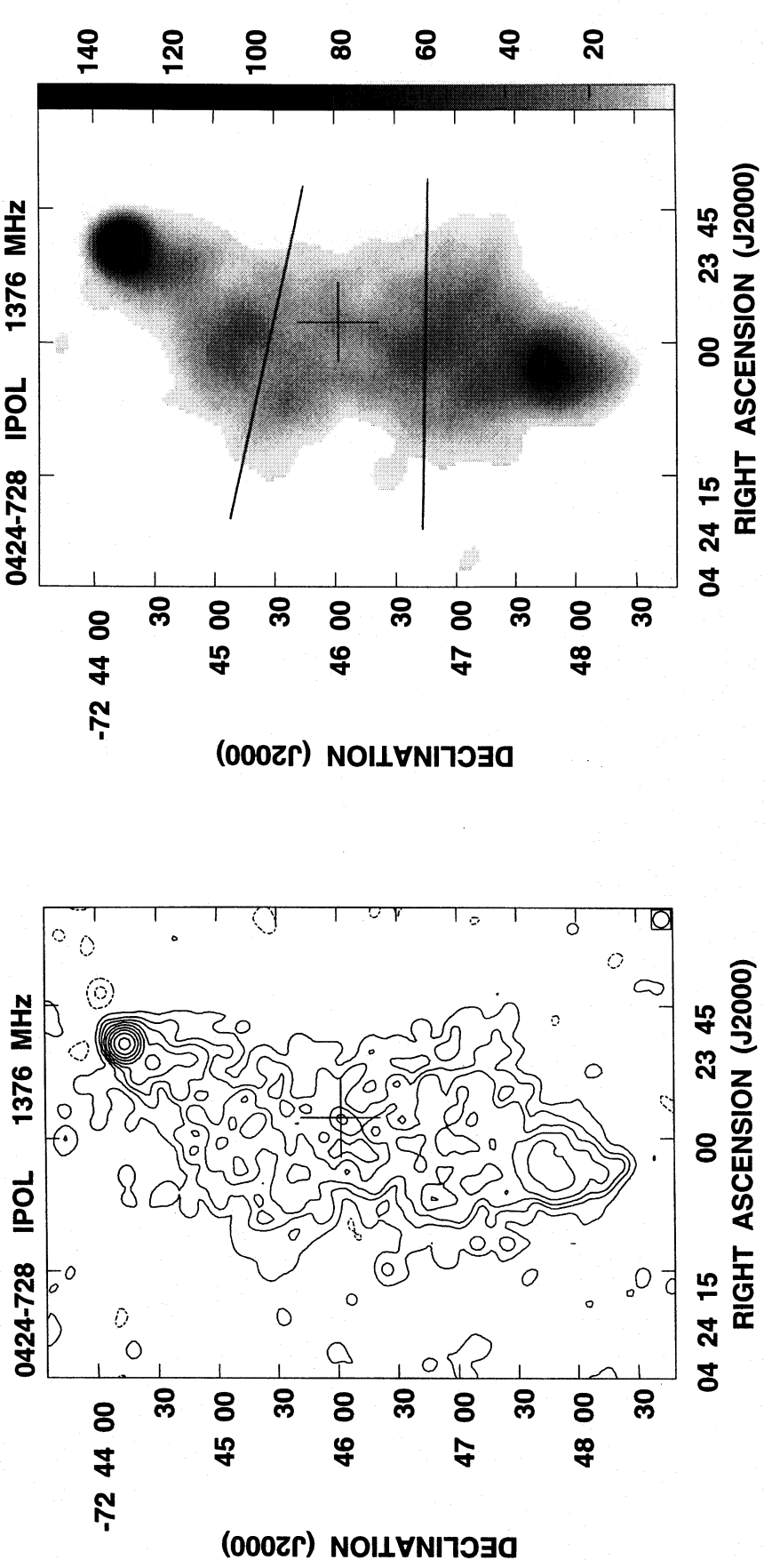

Figure 3. 1376-MHz images of 0424 − 728, as for Fig. 1. Contours are at 1 mJy beam^{-1} × (− 2, − 0.5, 0.5, 2, 4, 8, 16, 32, 64, 128, 256), and the beam size is 8 arcsec FWHM. The grey-scale spans the range 0.5–150 mJy beam^{-1} with a beam of 15 arcsec FWHM.

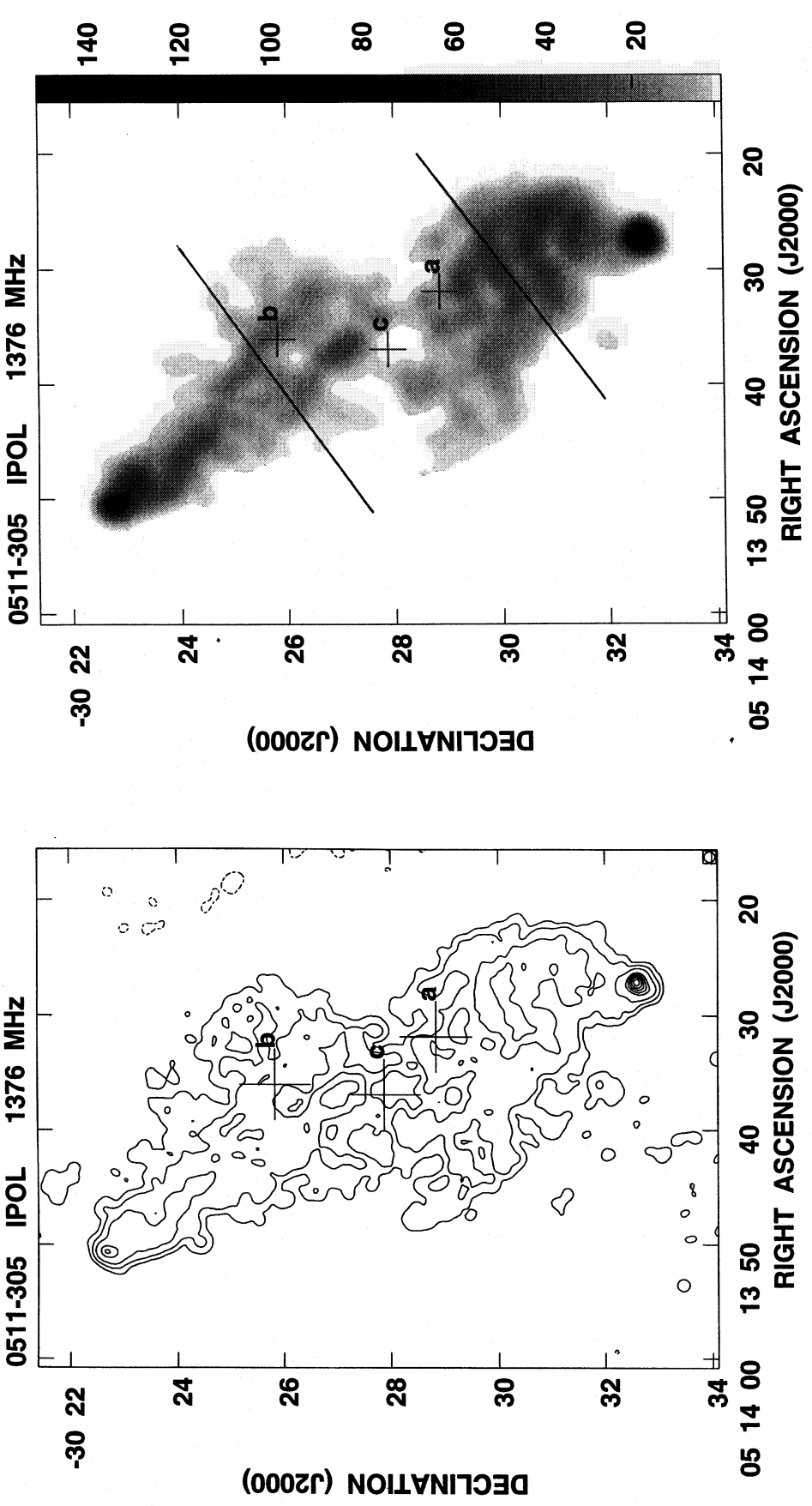

Figure 4. Images of 0511 − 305 in the form of (a) 1376-MHz contours, (b) 1376-MHz grey-scale, and (c) optical grey-scale. Contours are at 0.5 mJy beam^{-1} × (−1, 1, 4, 16, 64, 96, 128, 160, 192, 224), and the beam size is 12 arcsec FWHM. The grey-scale in (b) covers the range 1–150 mJy beam^{-1}, with a beam smoothed to 20 arcsec FWHM. The optical image of the parent galaxy is from the NASA/STScI digitized version of UK Schmidt IIIaJ plate 423, smoothed with a 2-arcsec Gaussian; the intensity scale is arbitrary.

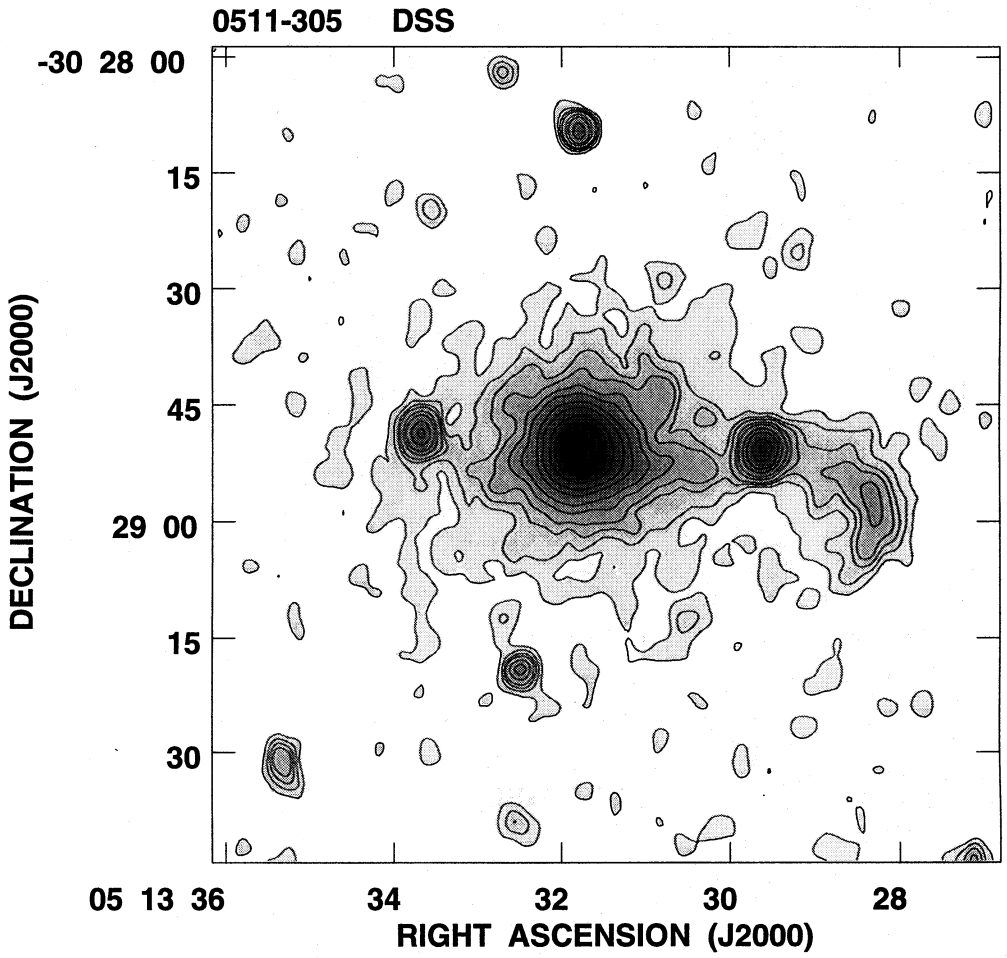

Figure 4 – *continued*

nal to the source axis. The lobes connect the hotspots to the core to form a continuous, but non-uniform, bridge. There are extended regions of enhanced brightness in both lobes which are recessed from the hotspots and symmetrically located, straddling the central engine. The axis through these high-surface-brightness lobe regions makes an angle of about 25° with respect to the line joining the bright outer hotspots.

The brightness enhancements in the lobes may be the sites of past hotspots. There is a diminution of brightness between these regions and the sites of current hotspots and, therefore, we hypothesize that the source was 'born again' with the current axis following an interruption in its activity. The misalignment of 25° between the current source axis, defined by the hotspots at the extreme ends of the source, and the axis in the previous phase of activity, defined by the resolved brightness enhancements in the lobes, may be indicating that the activity has resumed with a new ejection axis.

Whereas the older resolved lobes are symmetric about the core, the current hotspots are asymmetric and misaligned, possibly a consequence of light travel-time effects. The hotspots towards the south-east lie further from the core and consequently may represent a structure at a later epoch as compared with the north-west hotspot. With respect to the 'older' axis joining the recessed brightness enhancements in the lobes, the south-east axis makes a larger angle as compared to the north-west axis. This observation, together with the finding of multiple hotspots at the south-east extremity which are aligned orthogonal to the source axis, indicates that the ejection axis might be changing in a clockwise direction on the sky in successive periods of activity.

4.6 1545 – 321 (Fig. 6)

This giant source has a very unusual morphology in that the brightest unresolved hotspots are located well recessed from the ends of the lobes. On the sky plane, these hotspots are collinear with the position of the suggested optical identification and symmetrically placed on either side of the ID. There is a continuous bridge along the entire source and the lobes are brightened towards the source extremities. A curving ridge of emission connects the south-east hotspot with the south-east extremity of the source.

The location of hotspots close to the core is suggestive of FR I class morphology; however, the source is overall edge brightened and has a radio power that places it in the FR II category. It is, nevertheless, interesting that this source has one of the lowest radio powers in our sample.

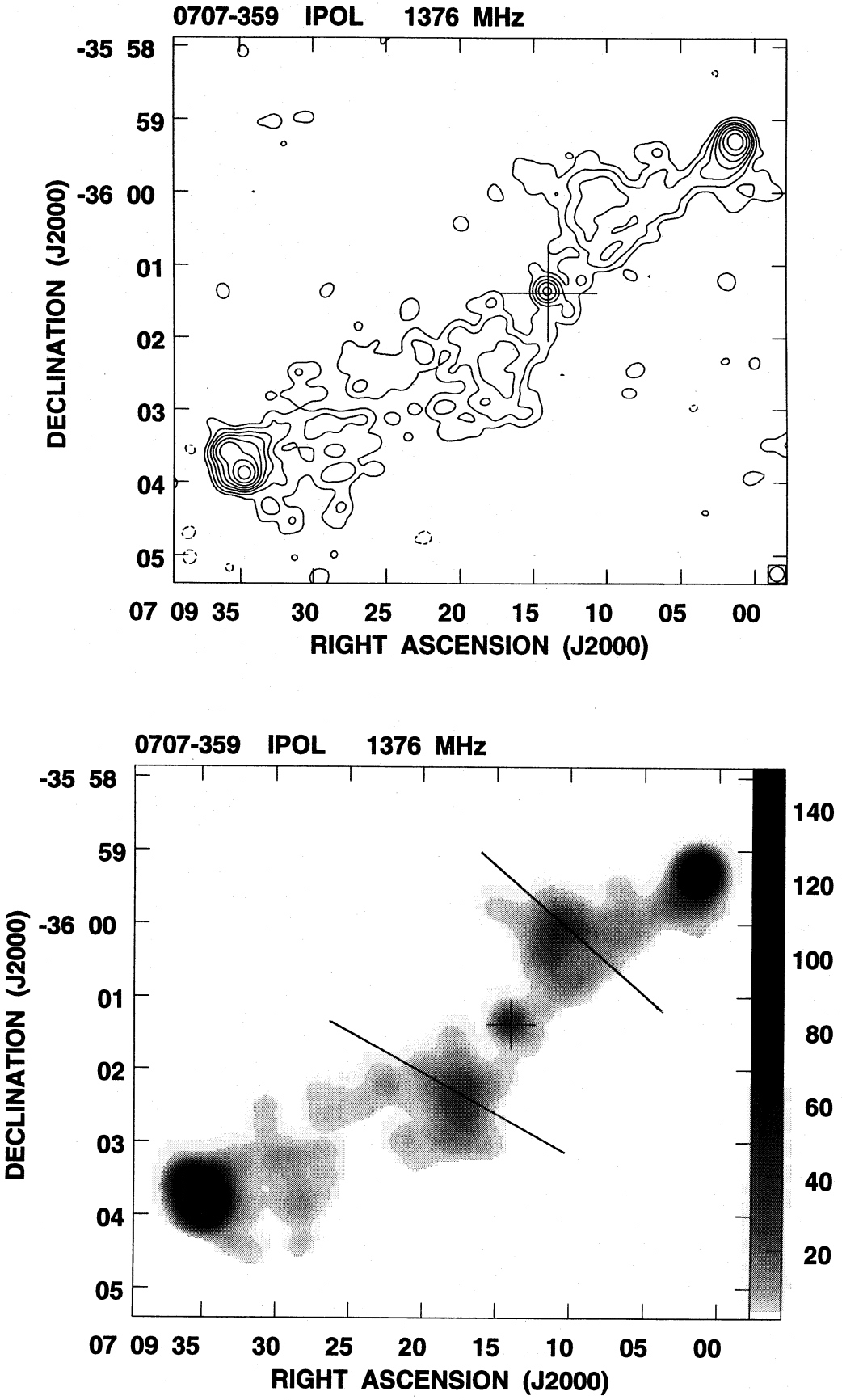

Figure 5. 1376-MHz images of 0707 – 359, as for Fig. 1. Contours are at 1 mJy beam^{-1} × (– 1, 1, 3, 8, 16, 32, 64, 128, 256), and the beam size is 12 arcsec FWHM. The grey-scale spans the range 2–150 mJy beam^{-1} with a beam of 20 arcsec FWHM.

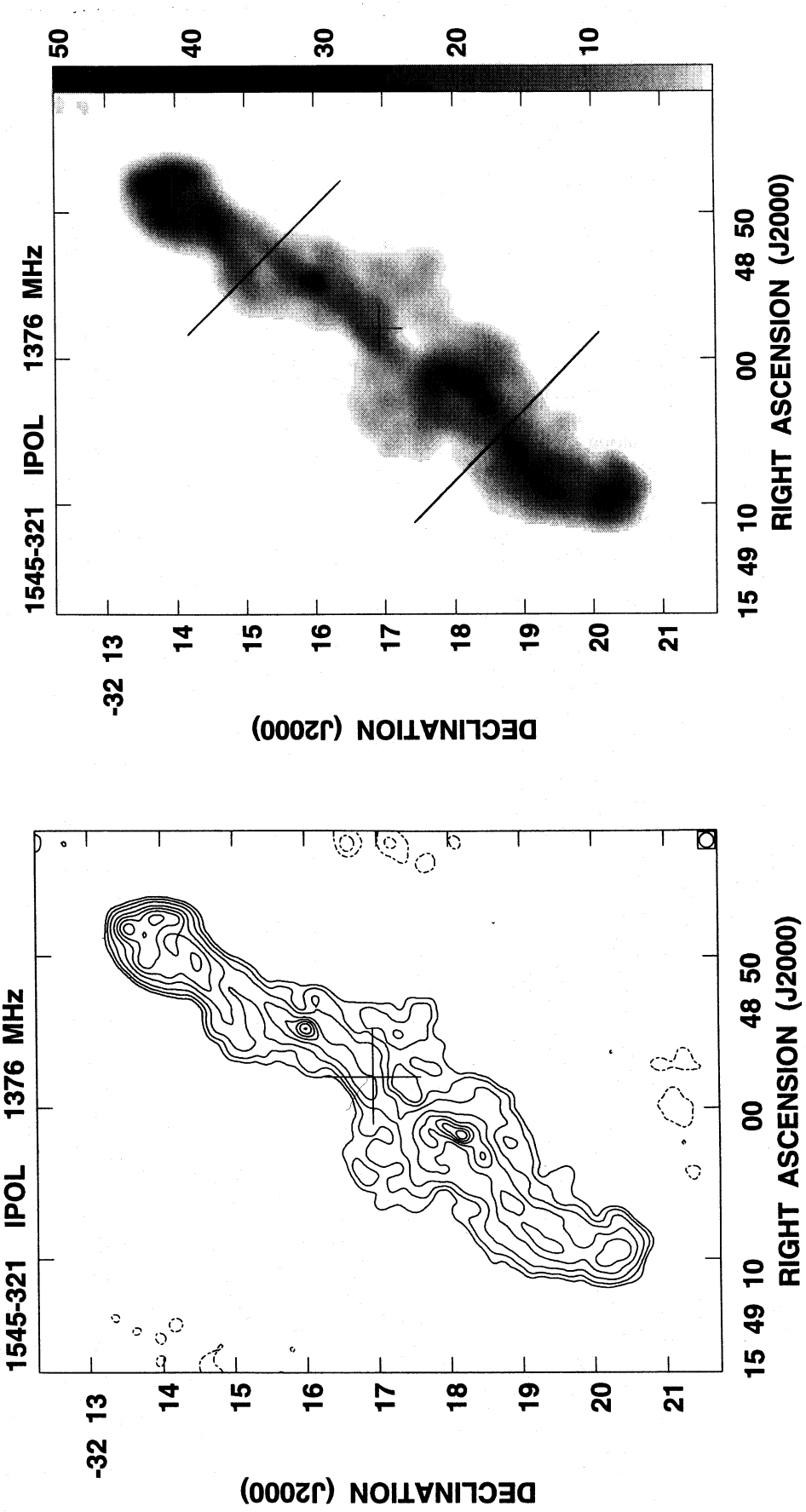

Figure 6. 1376-MHzz images of 1545 − 321, as for Fig. 1. Contours are 1 mJy beam^{-1} × (− 2, − 1, 1, 2, 4, 8, 12, 16, 20, 24), and the beam size is 12 arcsec FWHM. The grey-scale spans the range 0.5–50 mJy beam^{-1} with a beam of 15 arcsec FWHM.

The edge-brightened structure suggests that the beams must have been depositing their power at the ends at some time in the past. The present absence of hotspots at the ends, together with the detection of hotspots closer to the core, is indicative of restarted activity following an interruption. Hotspots are generally expected to form at the interface between beams and the ambient medium, and not within pre-existing cocoons. This would imply that the present activity has a new axis and that the observed hotspots are located at the cocoon walls; however, such a hypothesis would require a close alignment between the current and older axes as projected on the sky.

4.7 1910 − 800 (Fig. 7)

This source has the typical morphology of FR II class objects: there are hotspots at both ends, a core component, and tails directed from the hotspots and along the source axis towards the core. We detect a core component but it is not coincident with the optical ID proposed by JM. While there is nothing visible at the core position on the UK Schmidt IIIaJ film, inspection of the ESO R film copy shows a faint galaxy ($m_R \approx 20$) coincident with the radio core. As noted later, this field is probably obscured, with patchy nebulosity over much of the plate. The radio emission is axially symmetric and there are emission gaps on both sides of the core: we have not detected a continuous bridge. As was the case for 0211 − 479, there are minima in brightness between the lobes and the hotspots.

We have measured the redshift to be $z = 0.346$ from a low-resolution spectrum of the host galaxy obtained by one of us (RWH) at the Anglo-Australian Telescope. 1910 − 800 is, therefore, a relatively distant example of a giant radio galaxy and detailed follow-up observations of the source are in progress.

4.8 2356 − 611 (Fig. 8)

This source has the highest radio power in our sample. The morphology comprises unresolved hotspots at the extremities, short and bright tails directed from the hotspots towards the centre (these constitute the heads of the radio source), and a continuous bridge connecting the two heads.

There is a prominent extension to the west from the north-west lobe which is directed off the main source axis and appears to be aligned with the position of the core. This extension has no obvious oppositely directed counterpart, which might be expected if the structure traces the radio axis in a past phase of activity.

5 ENVIRONMENTS

A previous study of the distribution of optical galaxies in the fields of giant radio sources has suggested that the environment may be responsible for asymmetries in radio morphologies (Saripalli 1988). We have used the COSMOS digitized southern sky data base (Yentis et al. 1992), listing objects down to $b_J \approx 22.5$ from the UK Schmidt IIIaJ plates, to examine the density of galaxies in the vicinity of the radio galaxies in our sample. An object listing for the field of

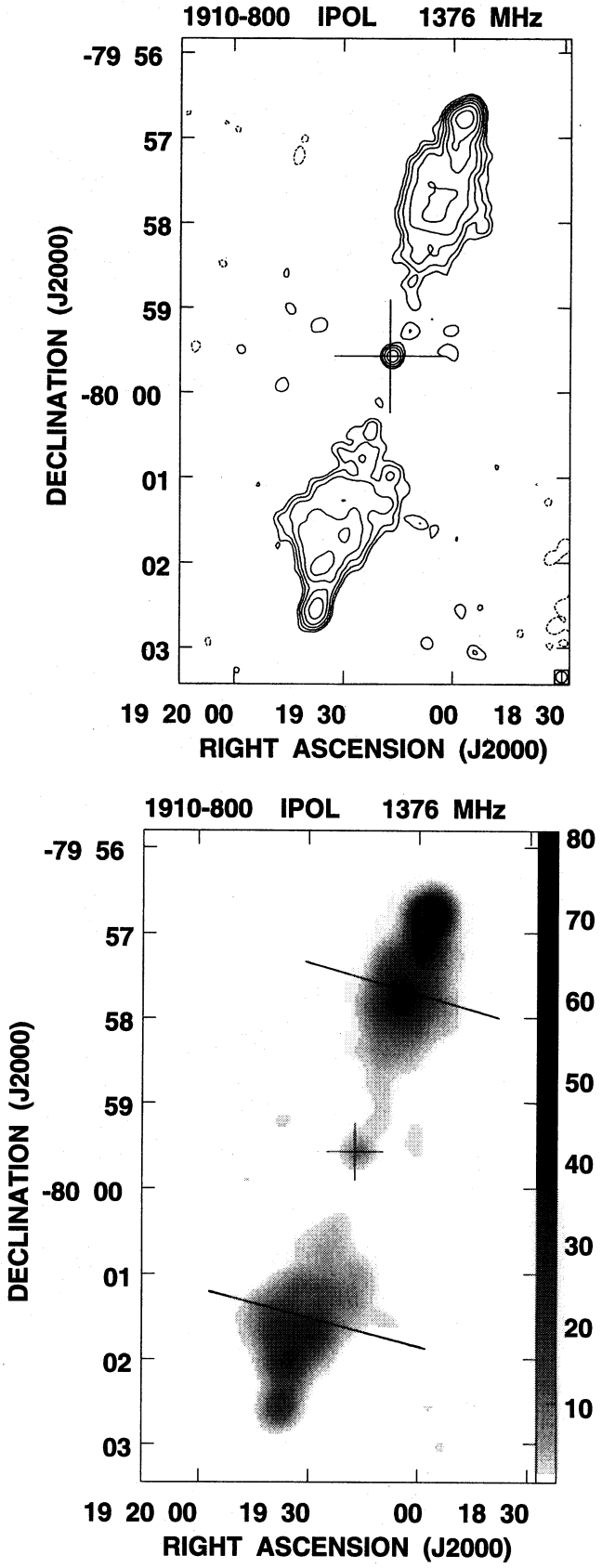

Figure 7. 1376-MHz images of 1910 − 800, as for Fig. 1. Contours are at 1 mJy beam^{-1} × (−1, −0.5, 0.5, 1, 2, 4, 8, 16, 32), and the beam size is 8 arcsec FWHM. The grey-scale spans the range 0.5–80 mJy beam^{-1} with a beam of 15 arcsec FWHM.

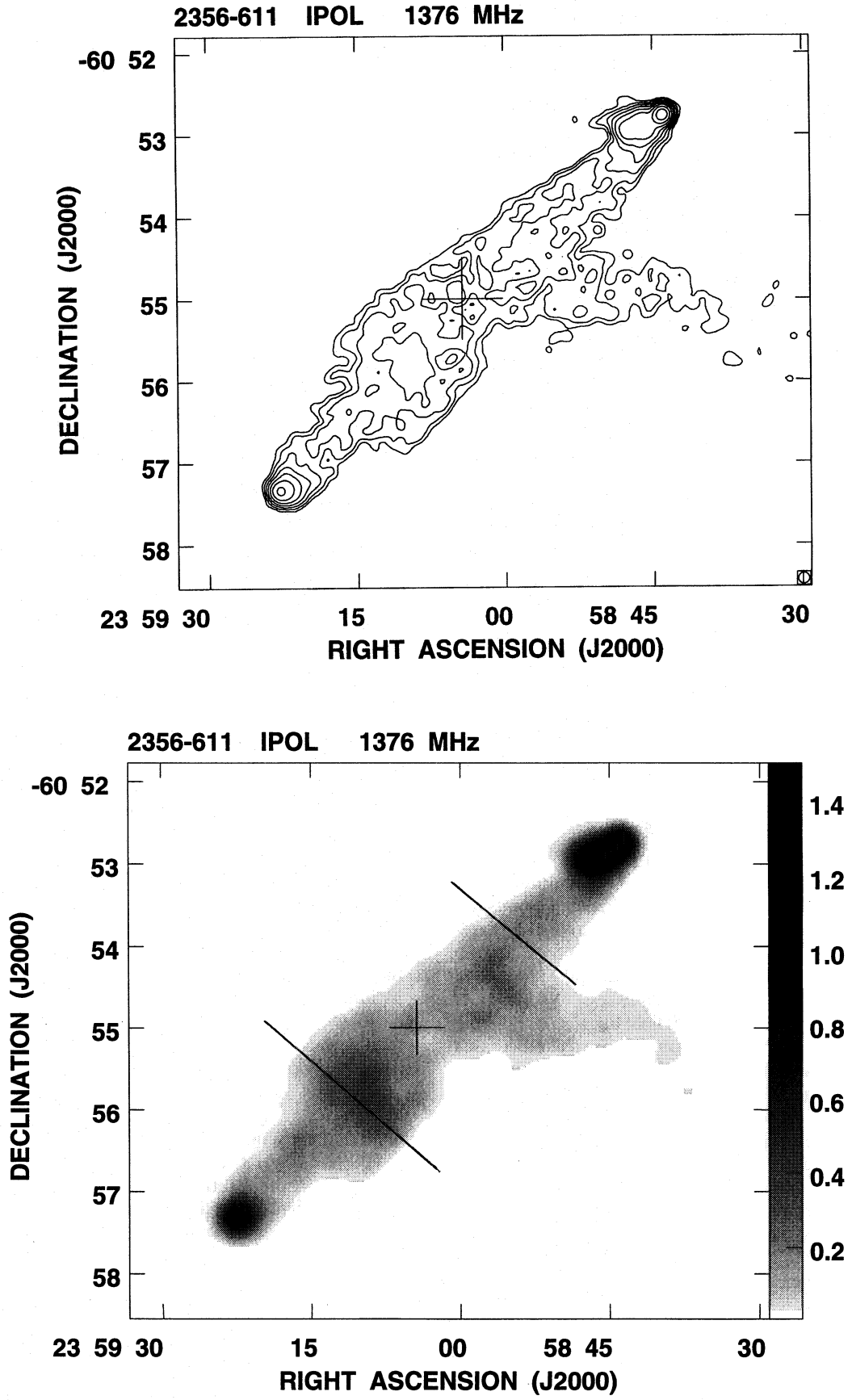

Figure 8. 1376-MHz images of 2356 – 611, as for Fig. 1. Contours are at 10 mJy beam^{-1} × (1, 2, 4, 8, 16, 32, 64, 128, 256), and the beam size is 8 arcsec FWHM. The grey-scale spans the range 0.015–1.5 Jy beam^{-1} with a beam of 15 arcsec FWHM.

Table 3. Galaxy counts in the fields of the radio galaxies.

Source	COSMOS b_J mag. of ID	Search mag. range b_J	Number of gal. counted, n	Mean number expected, $\bar{n}$	$\Delta n/\bar{n}$
0114−476	17.24	15.24–19.24	12	4.7	1.55
0211−479	19.07	17.07–21.07	6	8.9	−0.33
0511−305	16.7	14.70–18.70	7	3.2	1.19
0707−359	20.47	18.47–21.50	16	28.4	−0.44
1545−321	18.22	16.22–20.22	42	5.9	6.12
		20.22–21.50	40	23.9	0.67
1910−800	> 22	20.00–21.50	1	14.2	−0.93
2356−611	16.75	14.75–18.75	9	1.3	5.92
		18.75–21.50	14	26.7	−0.48

0424 − 728 was not available because of its proximity on the sky to the Large Magellanic Cloud; such regions of high star density are currently excluded from the COSMOS object catalogue. Listing of all objects classified as galaxies were extracted for the other seven fields. For 1910 − 800, however, where the identification is not visible on the IIIaJ survey plate, all objects down to the limiting magnitude were extracted, regardless of classification. In every field, we searched a circular area with radius equal to the distance between the host galaxy and the furthest extremity of the radio source, and counted the number of galaxies within ± 2 mag of the identification ($m_{\rm ID}$). A magnitude of 21.5 was adopted, however, as the limit at which the identifications were complete, i.e. the magnitude range was from $m_{\rm ID}-2$ to the smaller of $m_{\rm ID}+2$ and 21.5.

The expected numbers of galaxies in the field were estimated by a fit to the differential source counts around $b_{\rm J}=20$ using the compilation of Glazebrook et al. (1994). The fit yielded an integral source count of

$$N(<m)=10^{-7.038+0.4736m}\ \text{galaxies deg}^{-2}. \quad (1)$$

The numbers of galaxies counted in each field (n) within specific magnitude bins (in COSMOS $b_{\rm J}$ magnitudes) are listed in column 4 of Table 3; the mean expected counts ($\bar{n}$) in the same sky areas and magnitude ranges are listed alongside in column 5. Adding the expected numbers for the seven fields and comparing with the total galaxy count in these seven fields, we find a fractional excess, $(\sum n/\sum\bar{n})-1$, of 0.4. If we exclude the 1910 − 800 field because of possible obscuration in this direction, the fractional excess increases to 0.75. The mean excess in our observed fields as compared with expectation may be because our fields are centred on a galaxy (the optical ID of the radio source), and galaxies are known to be clustered (cf. Peebles 1993).

The fractional excess counts $\Delta n/\bar{n}$ (where $\Delta n=n-\bar{n}$) computed for the individual fields are listed in column 6. These estimates of the fractional excess in galaxy counts in the vicinities of the radio sources will suffer from errors primarily because the counts in column 4 are made in apparent magnitude bins (instead of real space) and because of COSMOS misclassifications (Unewisse, Hunstead & Piestrzynski 1993). Five fields (0114 − 476, 0211 − 479, 0511 − 305, 0707 − 359 and 1910 − 800) have $|\Delta n/\bar{n}|<2$. The remaining two fields (1545 − 321 and 2356 − 611) appear to show strongly enhanced galaxy counts, with $\Delta n/\bar{n}\sim 6$. If, however, we choose fainter magnitude bins which exclude the optical ID, these two fields have $\Delta n/\bar{n}<1$, indicating that the excess in each field may be local to the radio galaxy environment. Counts for the 1910 − 800 field are below expectation, even if we include objects too faint to be classified reliably as stars or galaxies: in the magnitude range 20–22.5, 14 objects are counted where at least 42 are expected. It is likely that the 1910 − 800 field is obscured, as noted above.

The morphologies of the giant radio galaxies may be influenced by their IGM environments. If galaxies are considered as tracers of the IGM, then the galaxy counts in the neighbourhood of the radio structures could be used to estimate the local IGM density. It should be cautioned here, however, that the use of $\Delta n/\bar{n}$ as an indicator of the fractional density contrast $\Delta\rho/\bar{\rho}$ of the IGM will involve an additional error due to the joint distribution of n and $\rho_{\rm IGM}$.

Of the seven sources whose optical fields have been examined, 1545 − 321 and 2356 − 611 have the most uniform bridges in the sample and also have no emission gaps. As discussed above, these are the two fields with significant excesses in galaxy counts and it appears, therefore, that an extreme environment may be responsible for this morphology. First, a higher ambient density, and consequently higher density contrast between the beam and IGM, may be expected to result in a decreased entrainment of IGM material at the head (Norman et al. 1982). Entrainment of thermal material adds inertia to relativistic plasma, reduces its internal sound speed and consequently slows down the backflow. These effects could explain the gaps in emission seen between the cores and lobes of sources located in low-density environments, as well as the increased contrast in bridge emission. Therefore, we may expect sources located in high-density gaseous environments to have less entrainment and consequently greater uniformity in bridge brightness. Secondly, a higher IGM density could imply a reduction in the lateral expansion velocities in lobes and consequently a reduction in the expansion losses in the lobes. As a result, we might expect any backflow to be more efficient in reducing the contrast in the bridges of such sources.

The lobes of these giant sources are expected to be overpressured with respect to the ambient intergalactic medium (Subrahmanyan & Saripalli 1993). Therefore, the lobe expansion and the head advance may both be ram pressure limited by the ambient density. Consequently, we may expect the axial ratio (see Section 6) to be unaffected by the density of the source environment. This is indeed the case:

1545 – 321 and 2356 – 611 have axial ratios similar to the remainder of the sample (see Table 2).

The indications of a relationship between the radio morphology and environment, where the environment density has been estimated by simple galaxy counts in magnitude ranges around the parent galaxies, suggest that it may be useful to examine the galaxy environments in greater detail through wide-field fibre-optic spectroscopy.

6 AXIAL RATIOS

We have computed the axial ratios of the eight sources by using the prescription given by Leahy & Williams (1984; hereinafter LW). The widths of the lobes are measured halfway between the core and the ends of the radio source and are taken to be $2/\sqrt{3}$ times the deconvolved half-power width. The axial ratios of the northern and southern lobes (R_N and R_S) are computed separately from the total extent and width of each lobe. The overall axial ratio for each source, R_T, is defined as the ratio of the total source extent to the average of the widths of the two lobes. The axial ratios for the individual sources are listed in Table 2. The median value of R_T is 5.6 and the median linear size is 1.5 Mpc.

A comparison sample containing smaller-size FR II type sources in the field, with radio powers similar to the sources in our sample, was constructed from the sample of LW. All sources which were deemed by Smith & Spinrad (1980) to be associated with clusters, unidentified sources, and those with linear extents exceeding 1 Mpc were omitted. The resulting sample of eight sources has a median linear size of 420 kpc and a median R_T of 5.0; the radio powers at 1376 MHz fall in the range $4–110 \times 10^{24}$ W Hz^{-1} sr^{-1}. The giant sources presented in this paper have linear sizes $\gtrsim 1$ Mpc, but similar radio powers, distributed in the range $4–80 \times 10^{24}$ W Hz^{-1} sr^{-1}. The sources in the two samples have similar redshift distributions: the median redshift in the LW sample is 0.19 and that in the giant sources sample is 0.17. Within the errors in the R_T estimates, it appears that the axial ratios are similar in the two samples.

The similarity in axial ratios between the small-sized comparison sources and the giants is indicative of self-similarity in the morphological evolution of FR II radio galaxies and of radio powers remaining fairly constant as the sources evolve to larger sizes. It may be noted here that the axial ratios in sources with *higher* powers (and with extents $\lesssim 1$ Mpc) are observed to be higher (Leahy et al. 1989): the median R_T for the field radio galaxies in their sample is ≥ 9.5. It would be interesting to examine the axial ratios in giant sources with high powers: unfortunately high-power giant radio galaxies are very rare.

If double radio sources of similar radio powers have morphologies which scale with linear size, a sample restricted to sources with extremely large projected linear sizes might be expected to have larger axial ratios than a sample restricted to small sizes simply because the larger sources have orientations biased to be close to the sky plane. The large- and small-sized source samples have, however, similar R_T, possibly because all the sources are radio galaxies. This selection effect may bias both samples against sources making small angles to the line of sight (Barthel 1989). As a result, our inference of similarity in R_T amongst sources with linear extents 200–2000 kpc may not be significantly influenced by orientation biases.

7 ENERGY DENSITIES IN THE LOBES

We have estimated the energy densities in the lobes of the sources at locations mid-way between the hotspots (or source extremities) and the core (or inner boundary of the detected lobe). Profiles of the intensity distribution were made along the sections marked across the lobes in Figs 1(b)–8(b), and the energy densities were estimated from the peak intensities, assuming that the line-of-sight depth is the deconvolved full width of the sections. Standard minimum-energy assumptions were made (Miley 1980), the filling factor was assumed to be unity and the energy was assumed to be carried solely in light radiating particles (electrons and/or positrons). The lobe spectral indices were estimated from our flux-density measurements at 1376 to 843 MHz, and the emission spectra were assumed to have low- and high-frequency cut-offs at 0.01 and 15 GHz, respectively. For each source the estimated energy densities at the profiles across the northern and southern lobes, u_N and u_S, and their average, u_T are listed in Table 2. The median of the eight u_T values is 8×10^{-14} J m^{-3}.

Adoption of the same assumptions and similar methodology enables us to estimate the energy densities in the field radio galaxies with $D < 1$ Mpc from the sample of LW. These sources have a median u_T of 5×10^{-13} J m^{-3}. It appears, therefore, that the lobes in the giant-sized sources, with a median extent of 1500 kpc, have energy densities ≈ 7 times lower than a sample of sources with a median extent of 420 kpc.

A radio source with a linear extent a and width b will have an axial ratio $R_T \sim a/b$, and consequently its volume V will scale as $V \sim a^3/R_T^2$. If the total energy is assumed to be a minimum, the energy, U, in relativistic particles scales with the radio power P as $U \sim P^{4/7}V^{3/7}$ (Moffet 1975). If we assume further that sources have continuous and uniform bridges, the energy density u may be expected to scale as

$$u \sim \left(\frac{PR_T^2}{a^3}\right)^{4/7}. \qquad (2)$$

Since our sample of giant radio galaxies and the LW comparison sample have similar radio powers and axial ratios, equation (2) predicts that the factor of 3.6 increase in size between the two samples should be balanced by a decrease in lobe energy density by a factor of 9. This is consistent with the observed decrease of a factor of 7, taking into account the errors in the median energy densities.

In Fig. 9, we have plotted P_{1376}/D^3 versus $u_T^{7/4}$ for the two samples. A line of slope unity, predicted by equation (2) for constant R_T, has been fitted to the sample of smaller sources. Among the giant sources, 1545 – 321 deviates most strongly from the extrapolation of the line to smaller u_T. The bridge surface brightness in this source may, however, be overestimated because of the prominent ridge line along the bridge. Even excluding this source, the giant sources appear to deviate marginally from the extrapolation, in the sense of having slightly higher lobe energy densities than predicted by equation (2). The similarity in axial ratios

between the two samples suggests that this deviation may arise from the larger sources having smaller filling factors for the synchrotron plasma in their lobes. Excluding 1545 − 321, we note that 0114 − 476, 0707 − 359 and 1910 − 800 appear to have the largest deviations in the sense that their lobe energy densities are in excess of that predicted by the extrapolation. They are also the three sources in the sample without continuous bridges. This leads us to infer that, in contrast to the smaller-sized sources, the giant sources tend to have emission gaps: their bridges are not always as continuous as in the smaller-sized sources. The occurrence of docked bridges among the giant sources may explain why they appear to have smaller filling factors in the lobes.

8 DISCUSSION OF SOURCE MORPHOLOGIES

8.1 Interaction with the intergalactic medium

Profiles of the emission intensity across the lobes of the giant sources in our sample usually show sharp cut-offs at the lobe boundaries. Since the lobes extend well beyond the coronal haloes which are commonly observed surrounding isolated elliptical galaxies, we expect them to be in direct interaction with the intergalactic medium (IGM). As discussed by Subrahmanyan & Saripalli (1993), *COBE* limits on the electron pressure in any uniform IGM suggests that the lobes of giant radio sources are overpressured with respect to the ambient gas. The sharp boundaries are, therefore, indicative of ram pressure confinement of the laterally expanding lobes. Consequently, we may infer that the sound speed in the lobe exceeds the lateral expansion velocity.

The similarity in R_T between the present giant sample and that of LW indicates that, if radio galaxies evolve with fairly constant radio powers, the lobes must grow laterally at a rate proportional to the velocity of advance of the heads into the IGM. The constant of proportionality would be the source axial ratio. The implied self-similar growth is consistent with commonality in the physics of the interaction between the heads and lobes with the IGM environment: both forward and lateral advances are ram pressure confined.

We observe filamentary structure in many of the giant galaxy lobes. The sound speed in the lobe synchrotron plasma may be relativistic ($\sim c/\sqrt{3}$) and may well exceed the lobe expansion speed (which is a factor of R_T below the head advance speed); therefore, we might expect these filamentary structures to be transient features with lifetimes shorter than the lobe expansion time-scales. On the other hand, if bulk velocities in the cocoon are reduced (below the $c/\sqrt{3}$ expected in a relativistic plasma) due to any entrainment of thermal IGM plasma at the head, the lifetimes of the filamentary structures may approach the lobe expansion time-scales.

8.2 Cause for departures from axial symmetry

Displacements of the lobes from the source axis have been commonly observed in smaller sources (LW) and often interpreted as arising from an interaction between the halo surrounding the parent galaxy and the backflowing cocoon.

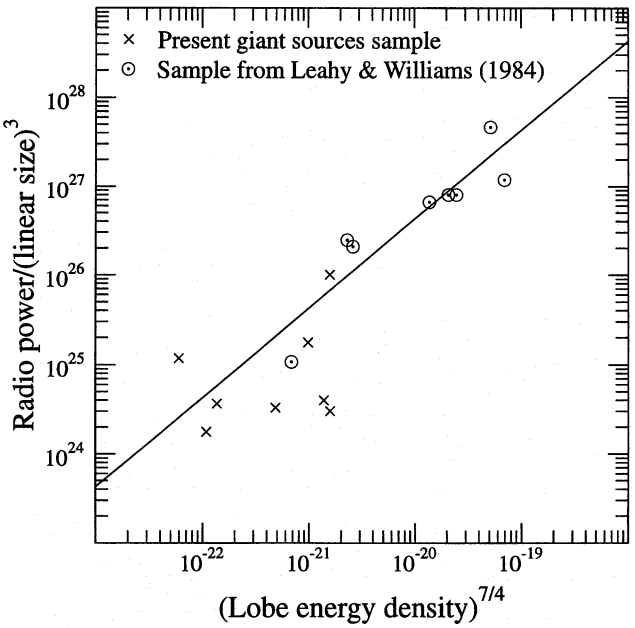

Figure 9. Relationship amongst radio power, linear size and lobe energy density for the present giant source sample and the LW sample with $D < 1$ Mpc, with the aim of testing the simple model of equation (2). The ordinate is the ratio of the 1376-MHz radio power to the cube of the linear size of each source, and the abscissa is the (7/4)th power of the energy density in the synchrotron plasma of the lobes. The plot has logarithmic axes and the straight line is a least-squares fit of a line of slope unity to the points from the LW sample.

Several of the giant sources being presented here have offset lobes: 0114 − 476, 0211 − 479 and 0424 − 728 are examples where the lobe deviates from the source axis on one side; 0511 − 305 and 0707 − 359 show deviations from the source axis on both sides and are inversion symmetric; the remaining three sources may be considered to have axial symmetry. The displacements and bends from the source axis are, however, observed to occur several hundred kpc from the parent galaxy, well beyond the scale of X-ray haloes commonly observed in early-type galaxies. The linear scales of the deviations indicate that the distortions arise due to transverse velocities comparable in magnitude to the head advance speed. The departures from axial symmetry that we observe in the morphologies of the giant sources are similar to the distortions observed in smaller sources by LW, and the fraction of sources showing such distortions (5/8) is also similar to that found by LW (two-thirds). The morphologies appear to be self-similarly scaled from those of the smaller sources, i.e. the deviations from the source axis do *not* occur at similar linear distances from the parent galaxies in the two samples.

If the coronal haloes have a characteristic scale of about 100 kpc, corresponding to their maximum observed extents (Forman et al. 1985), it is unlikely that cocoon–halo interactions are the cause of the observed off-axis deviations in the giant sources. Therefore, the LW hypothesis, that the deviations in their smaller-sized sources are due to such interactions, may not be applicable to giant sources. On the other hand, the indication that the distortions scale roughly

self-similarly from the smaller to giant sources leads us to infer that the structure of the ambient medium is also roughly self-similar. This suggests that the galaxy halo properties – density and temperature – may decline with distance from the central galaxy without any halo–IGM discontinuity or truncation.

Although the lobes show distortions, the hotspots and central engines are collinear in most cases and we do not observe any bent sources: the maximum angle between the lines joining the position of the optical ID to the brightest hotspots on either side is 20°. This observation is also true of the sources in the LW sample. The collinearity indicates that as sources evolve to larger size, they probably maintain a linear axis and consequently we may expect only inversion-symmetric distortions which may arise due to a changing beam axis, perhaps in different phases of central activity. Cases of one-sided distortions (notably in 0211 – 479 and 2356 – 611) are, however, also observed: the maximum bending angles observed in our sample and that of LW indicates that the observed one-sided distortions (and mirror-symmetric distortions observed in the LW sample) may not be caused by the source having a very bent morphology at an earlier epoch. As discussed in Section 4.2, departures from axial symmetry in the giant sources are also not likely to be due to movement of the parent galaxy with respect to the IGM or due to buoyancy effects in the IGM. These may be indicating that the backflowing cocoons are being deflected to produce such deviations. The linear size of the deflections would, however, now require that the backflowing cocoon plasma has significant bulk velocity, implying that the bulk kinetic energy in the beam has not been completely dissipated at the head. Evidence for *in situ* acceleration in the lobes (cf. Alexander 1987) supports this hypothesis.

8.3 Evidence for discontinuous beams

Several sources (0211 – 479, 0707 – 359, 1910 – 800 and 2356 – 611) appear to have a minimum in intensity between their compact hotspots and extended lobes; this phenomenon is particularly pronounced in the case of 0707 – 359. 0114 – 476 and 1545 – 321 show hotspots well recessed from the ends of the lobes. Both these characteristics may be signs of discontinuity in the beams and, perhaps, interruptions in the central activity.

Bridges have been found to be ubiquitous in <1 Mpc sized FR II sources (LW; Leahy et al. 1989). Our observations show, however, cases of >1 Mpc sized sources – notably 0114 – 476 – where the lobes are docked. Emission gaps are also observed in 0211 – 479 and 1910 – 800. As shown by the comparison in Fig. 9, the giant sources typically have less uniform bridges. This phenomenon may again be evidence for multiple epochs of activity leading to the formation of the giant-sized sources.

9 CONCLUSIONS

We have observed the radio structures in a sample of southern radio galaxies which are representative of the morphologies in giant radio galaxies, and made a comparison between their properties and that of smaller-sized sources. We infer that:

(i) the giant sources have axial ratios similar to those in smaller-sized sources with similar radio powers;

(ii) giant sources tend to have less uniform bridges as compared with these smaller-sized sources;

(iii) sources located in environments with higher galaxy densities, and presumably higher densities of the ambient IGM gas, tend to have more uniform bridges;

(iv) the deviations from axial symmetry in the giant sources are observed to be linearly scaled versions of the distortions observed in smaller sources;

(v) giant sources often show morphological indications for interruptions in the beams.

We conclude that FR II radio galaxies probably undergo self-similar morphological evolution with fairly constant radio powers. The structure in the lobes is probably influenced significantly by the physical nature of the ambient medium, with smaller sources and also the larger sources which are located in denser environments tending to have more uniform bridges. Emission gaps may be a characteristic of the largest sources which are located in the lowest-density parts of the IGM.

The morphological similarity between the off-axis distortions seen in the giant sources, as compared with smaller-sized sources, indicates that they may both have similar causes. While inversion-symmetric distortions can be explained by changing beam axes, a different explanation is needed for the observed one-sided distortions which imply that the lobe backflows are being deflected systematically. If the deflection were due in some way to the galactic halo, the structural similarities between sources differing by an order-of-magnitude in linear size suggests that the halo itself has no discontinuities and probably falls off smoothly with distance from the active nucleus.

Finally, we suggest that giant radio galaxies may have attained their large sizes as a result of a 'restarting' of their central engines in multiple phases of activity along roughly similar directions.

ACKNOWLEDGMENTS

The authors acknowledge the use of the Australia Telescope Compact Array (operated by the Australia Telescope National Facility). This research made use of the COSMOS/UKST Southern Sky catalogue as supplied by the Anglo-Australian Observatory. We thank Barbara Piestrzynski for reduction of MOST data, Paul Jones and Bruce McAdam for communications and Peter Scheuer and Wolfgang Kundt for discussions. We thank the referee for a useful suggestion. LS thanks the Alexander von Humboldt Stiftung for a post-doctoral fellowship, RS thanks the Forschungszentrum Jülich GmbH for financial assistance, and RWH acknowledges funding from the Australian Research Council.

REFERENCES

Alexander P., 1987, MNRAS, 225, 27
Baldwin J. E., 1982, in Andernach H., Wielebinski R., eds, Proc. IAU Symp. 97, Extragalactic Radio Sources,. Reidel, Dordrecht, p. 21
Barthel P. D., 1989, ApJ, 336, 606

Begelman M. C., Blandford R. D., Rees M. J., 1984, Rev. Mod. Phys., 56, 255
Black A. R. S., Baum S. A., Leahy J. P., Perley R. A., Riley J. M., Scheuer P. A. G., 1992, MNRAS, 256, 186
Bolton J. G., Clarke M. E., Ekers R. D., 1965, Aust. J. Phys., 18, 627
Ekers R. D., 1982, in Andernach H., Wielebinski R., eds, Proc. IAU Symp. 97, Extragalactic Radio Sources. Reidel, Dordrecht, p. 465
Ekers R. D., Goss W. M., Wellington K. J., Bosma A., Smith R. M., Schweizer F., 1983, A&A, 127, 361
Ekers R. D. et al., 1989, MNRAS, 236, 737
Fanaroff B. L., Riley J. M., 1974, MNRAS, 167, 31P
Forman W., Jones C., Tucker W., 1985, ApJ, 293, 102
Glazebrook K., Peacock J. A., Collins C. A., Miller L., 1994, MNRAS, 266, 65
Hine R. G., 1979, MNRAS, 189, 527
Jenkins C. J., McEllin M., 1977, MNRAS, 180, 219
Jones P. A., McAdam W. B., 1992, ApJS, 80, 137
Jones P. A., McAdam W. B., Reynolds J. E., 1994, MNRAS, 268, 602
Leahy J. P., Muxlow T. W. B., Stephens P. W., 1989, MNRAS, 239, 401
Leahy J. P., Williams A. G., 1984, MNRAS, 210, 929
Miley G. K., 1980, ARA&A, 18, 165
Miralda-Escudé J., Rees M. J., 1994, MNRAS, 266, 343
Moffet A. T., 1975, in Sandage A., Sandage M., Kristian J., eds, Stars and Stellar Systems vol. 9, Galaxies and the Universe. The Univ. of Chicago Press, Chicago, p. 211
Norman M. L., Smarr L., Winkler K. H., Smith M. D., 1982, A&A, 113, 285
Peebles P. J. E., 1993, Principles of Physical Cosmology. Princeton Univ. Press, Princeton
Saripalli L., 1988, PhD thesis, Indian Institute of Science, Bangalore
Saripalli L., Gopal-Krishna, Reich W., Kuhr H., 1986, A&A, 170, 20
Scheuer P. A. G., 1974, MNRAS, 166, 513
Schilizzi R. T., McAdam W. B., 1975, Mem. R. Astron. Soc., 79, 1
Searle L., Bolton J. G., 1968, ApJ, 154, L101
Smith H. E., Spinrad H., 1980, PASP, 92, 553
Subrahmanyan R., Saripalli L., 1993, MNRAS, 260, 908
The Australia Telescope, 1992, Special issue of J. Electr. Electron. Eng. Aust., 12, June
Unewisse A. M., Hunstead R. W., Piestrzynski B., 1993, Proc. Astron. Soc. Aust., 10, 229
Yentis D. J., Cruddace R. G., Gursky H., Stuart B. V., Wallin J. F., McGillivray H. T., Collins C. A., 1992, in McGillivray H. T., Thomson E. B., eds, Digitised Optical Sky Surveys. Kluwer, Dordrecht, p. 67